The Effects of NOAA-20 VIIRS Solar Diffuser Stability Monitor (SDSM) Relative Spectral Response (RSR) on the Solar Diffuser (SD) Degradation estimations

Taeyoung Choi[1,2*]

[1] Global Science & Technology (GST), Inc., 7855 Walker Dr., Suite 200, Greenbelt, MD 20770, U.S.A.
[2] NOAA Center for Satellite Applications and Research (STAR), 5830 University Research Ct., College Park, MD 20740-3818, U.S.A.

ABSTRACT

Solar Diffuser (SD) has been used for on-orbit imaging sensors such as historical Terra and Aqua Moderate Resolution Imaging Spectroradiometer (MODIS) and next generation NOAA's Visible Infrared Imaging Radiometer Suite (VIIRS) sensors. The SD provides radiometric calibration reference for Reflective Solar Bands (RSB) and it also carries ground calibration to on-orbit. There have been slight discrepancies in the long-term radiometric calibration using SD and moon. Even though there have been some studies and publications to explain these differences, the differences were assumed to be the viewing angle differences to the SD.

Using a Surface Roughness-induced Rayleigh Scattering (SRRS), we tested the current SD degradation estimation algorithms and found that the center wavelength based current SD estimation algorithm over-estimated SD degradations up to one percent level in the shortest wavelength band after two years of operation. Instead of using the center wavelength approach, the correct SD degradation was estimated by using the Relative Spectral Response (RSR) function of the SDSM detectors. After applying the correct SD degradation, the on-orbit calibration coefficients were very consistent with the moon based calibration.

Keywords: NOAA-20 VIIRS, RSB, Solar Diffuser, SRRS, RSR, SDSM

1. INTRODUCTION

The NOAA-20 Visible Infrared Imaging Radiometer Suite (VIIRS) was launched on November 18, 2017 successfully carrying the Advanced Technology Microwave Sounder (ATMS), Ozone Mapping Profiler Suite (OMPS) and Cross-track Infrared Sounder (CrIS) for weather prediction and environmental monitoring [1]. The VIIRS has 14 Reflective Solar Bands (RSB), one Day Night Band (DNB) and 7 Thermal Emissive Bands (TEB) covering spectral ranges of 0.41 to 2.25 μm for RSB, 0.5 to 0.9 μm for DNB, and 3.7 to 12.5 μm for TEBs with the spatial resolutions of VIIRS at the nadir angle of 750 and 350 meters for the Moderate resolution (M) bands and Imaging (I) bands, respectively [2-4].

The VIIRS instrument has on-board calibrators that are capable of National Institute of Standards and Technology (NIST) traceabilities with the extensive prelaunch calibration tests. Figure 1 shows VIIRS On-board Calibrators (OBCs) that are Solar Diffuser (SD), Solar Diffuser Stability Monitor (SDSM), Blackbody (BB), and Space View (SV). The SD is the main source of calibration for RSBs and DNB with the known and prelaunch measured Bidirectional Reflectance Distribution Function (BRDF), the BB is the primary calibration target for the TEBs with the known temperature and extremely low emissivity. Finally, the SV provides the zero signal responses by observing the deep space that are used for net detector response calculation by removing the offset of the detector with the SV counts.

For RSB calibration, the SD became the primary source of calibration for Earth Observing sensors such as VIIRS on S-NPP and NOAA-20 satellites, Moderate Resolution Imaging Spectroradiometer (MODIS) on Terra and Aqua satellites, Landsat Operational Land Imager (OLI), and Multi-angle Imaging Spectro-Radiometer (MISR) [5-9]. The SD also became a standard calibration source for the geo-stationary sensors Advanced Baseline Imager (ABI) on GOES R satellites and Advanced Himawari Imager (AHI) on Himawari 8 satellite [10, 11].

Earth Observing Systems XXVI, edited by James J. Butler, Xiaoxiong (Jack) Xiong, Xingfa Gu, Proc. of SPIE Vol. 11829, 118290W · © 2021 SPIE
CCC code: 0277-786X/21/$21 · doi: 10.1117/12.2593935

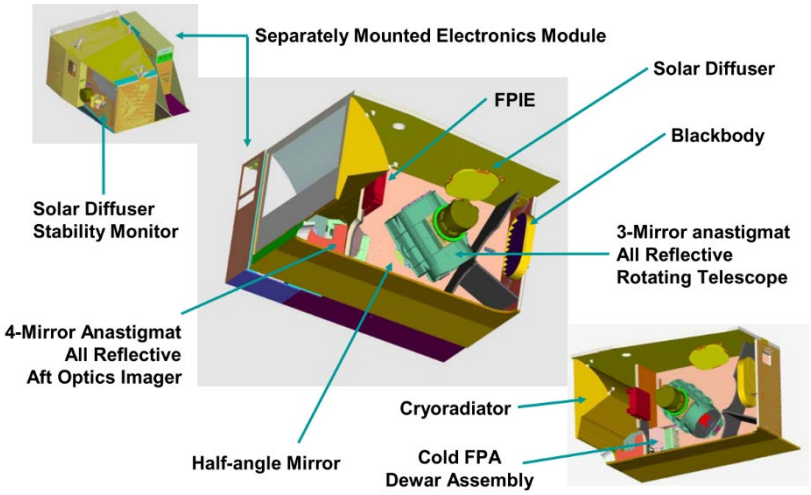

Figure 1. VIIRS opto-mechanical module (OMM) and On-Board Calibrator schematic [2].

There were viewing angle differences of the SD and moon through SV on to the primary mirror for Terra and aqua MODIS cases. The SD observations are made at an Angle Of Indices (AOI) of 50.2 degrees to the primary scan mirror whereas the middle of SV AOI was 10.2 with the lunar collections [12]. The two different responses were used to develop long-term Responses Versus Scan (RVS) responses especially for the Reflective Solar Bands (RSB). To resolve these two different AOI issues, VIIRS was intentionally built to have the same AOI of 60.4 degrees on to the Half Angle Mirror (HAM) at the center of the SD and SV view ports. By having the same 6.04 degrees AOI on the HAM, the long-term VIIRS SD and lunar calibrations are expected to have the same trends. But in reality, there were differences between the SD and lunar calibration for both S-NPP and NOAA-20 VIIRS [13-16].

To test (or mitigate) the long-term differences between the lunar and SD calibrations, the conventional SD degradation estimation method is tested with the NOAA-20 VIIRS RSB. A new SD degradation estimation method (called H_{RSR}) is developed using the Relative Spectral Response (RSR) function. The conventional center wavelength-based SD degradation (H-factor) is compared with the newly developed HRSR using the Surface Roughness-induced Rayleigh Scattering (SRRS) physical model [17]. In the short wavelength SDSM detectors, the SRRS simulation results show that there are up to 1.5 percent difference between the conventional H-factor and H_{RSR}. The newly developed H_{RSR} function was applied to the on-orbit radiometric calibration coefficient called F-factors. As an independent validation, the long-term lunar F-factor trends are compared with the updated SD F-factors and the new H_{RSR} function successfully reduced the radiometric calibration differences between the SD and lunar F-factors.

2. ON-ORBIT VIIRS RADIOMETRIC CALIBRATION

2.1 H-factor Algorithm (SD degradation estimation)

The SD is the on-orbit calibration reference and it degrades overtime because of the strong ultraviolet (UV) bombardment from the solar flux [17]. The SD degradation is measured by the Solar Diffuser Stability Monitor (SDSM) as shown in Figure 2. In the figure, SDSM measures alternating views of SD, dark, and Sun through the SD and SDSM attenuation filters. Basically, the H-factor is a time-dependent ratio between the Sun response as a reference in the denominator and the corresponding SD response in the numerator as shown in Equation 1.

$$H\text{-}factor(t) = \frac{dc_{SD}(t)\tau_{SDSM}}{dc_{SUN}(t)BRDF_{SDSM}\tau_{SDS}cos(\theta_{inc})\pi sin^2\varphi} \quad (1),$$

where dc_{SUN} is bias removed SDSM Sun view DC, τ_{SDS} is SD screen transmittance function, $BRDF_{SDSM\_SD}$ is the BRDF at the SDSM viewing angle to the SD surface, θ_{inc} is the solar incident angle to the SD screen, and $\pi sin^2\varphi$ is the solid

angle of the SDSM SD view port, dc_{SD} is bias removed SD view DC, and τ_{SDSM} is SDSM Sun screen transmittance. For NOAA-20 VIIRS, the initial H-factor showed large oscillations more than 1 % level in the longer wavelength SDSM detectors. It was caused by the prelaunch SDSM Sun transmittance LUT (τ_{SDSM}). The problem was resolved after applying a new τ_{SDSM} function to the H-factor [5, 18-20].

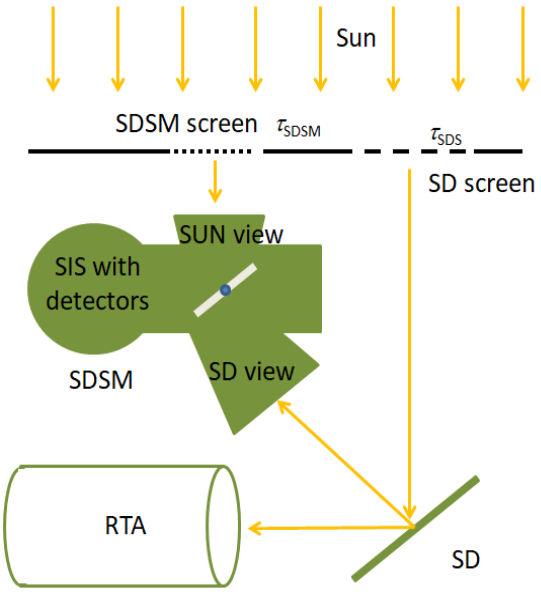

Figure 2. A simplified schematic of SD, SDSM and RTA relationship [5].

2.2 F-factor Algorithm (Sensor Calibration Coefficients)

The major on-orbit calibration is performed by the SD observations with the proper Sun illumination at the termination point near the South Pole. As a Sun-synchronous sensor in the descending node, NOAA-20 VIIRS can have 14 or 15 SD observations per day through RTA as shown in Figure 1 and 2. The F-factor is defined as

$$F\text{-}factor(t) = \frac{cos(\theta_{inc}(t))\left\{E_{sun}\tau_{SDS}BRDF_{RTA}\frac{H(t)}{H(t_0)}\right\}RVS_{SD}}{C_0+C_1dn_{SD}(t)+C_2dn_{SD}^2(t)+C_3dn_{SD}^3(t)} \quad (2)$$

Where $cos(\theta_{inc}(t))$ corrects the cosine effect of the incoming sun light, E_{sun} is the solar irradiance value in each band, the $\tau_{SDS}BRDF_{RTA}$ is SD Bidirectional Reflectance Distribution Factor (BRDF) through RTA view with SD screen effects, $H(t)/H(t_0)$ is normalized SD H-factor, RVS_{SD} is the Responses Versus Scan angle at the SD scan angle on the Half Angle Mirror (HAM), $c_{0\text{-}3}$ are the DN to radiance conversion coefficients with the electronics and detector temperature corrections from the prelaunch measurements, and dn_{SD} is bias removed DN from the SD observations. It should be noted that the H-factor is directly multiplied by the F-factor. This means that any changes in the H-factor estimation directly affects the F-factors and the VIIRS product radiance and reflectance.

3. H-FACTOR SIMULATION USING SURFACE ROUGHNESS RAYLEIGH SCATTERING (SRRS) MODEL

3.1 SRRS Model Fitting from the Fitted H-factors

Before the H-factor simulation, NOAA-20 VIIRS SD degradation (H-factor) is derived by the SDSM observations using Equation (1) as shown in Figure 3. It can be easily seen that the SD reflectance degradation is more pronounced in the short wavelength SDSM detectors (especially detectors 1 to 4).

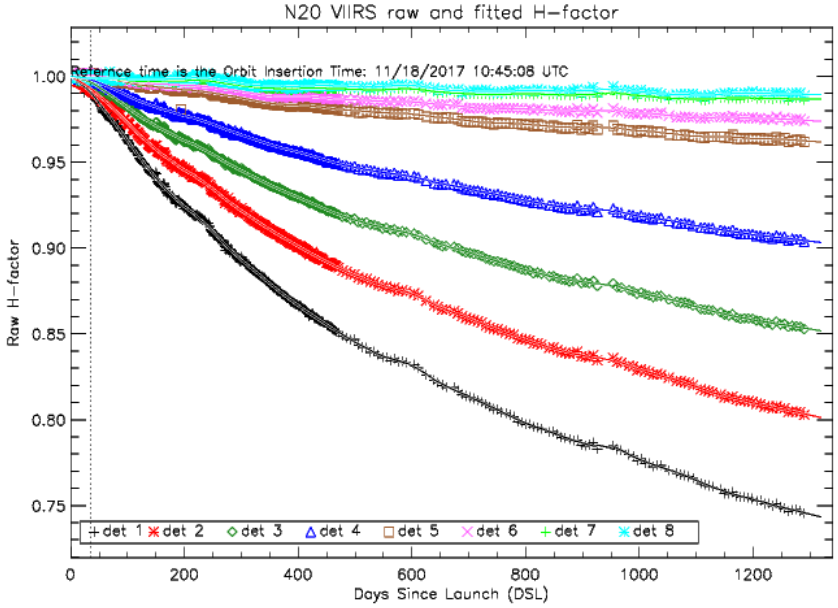

Figure 3. NOAA-20 VIIRS on-orbit SD degradation (H-factor) as of June 4, 2021.

The Surface Roughness Rayleigh Scattering (SRRS) model is numerically described in Equation (3) with the surface roughness factor *R(t)* and the order of the wavelength factor of *n*.

$$\frac{R(t)}{\lambda^n} = 1 - H(t,\lambda) \tag{3}$$

Detailed explanations of the SRRS model are well described by Shao's work [17] and the SRRS model was well fitted with the 4th order as shown in Equation (3) because the roughness correlation length is much smaller than the wavelength. As a result, more scattering is expected at the short wavelength.

Using the fitted H-factors (lines in Figure 3), the suggested fitting exponent is reaching order of 2 as shown in Figure 4 with the growing surface roughness factor R(t). The NOAA-20 H-factor is fitted to the model and the exponent *n* and *R(t)* in Figure 5 are derived over the wavelength fit using the forth order fit and the SDSM center wavelengths and time. The final SRRS model is describe in Equation 4 and 5 where

$$SRRS(t,\lambda) = 1 - \frac{R(t)}{\lambda^{4.0}} \tag{4}$$

and, $R(t) = 7.6259767e-06 * t - 9.1397806e-10 * t^2$. (5)

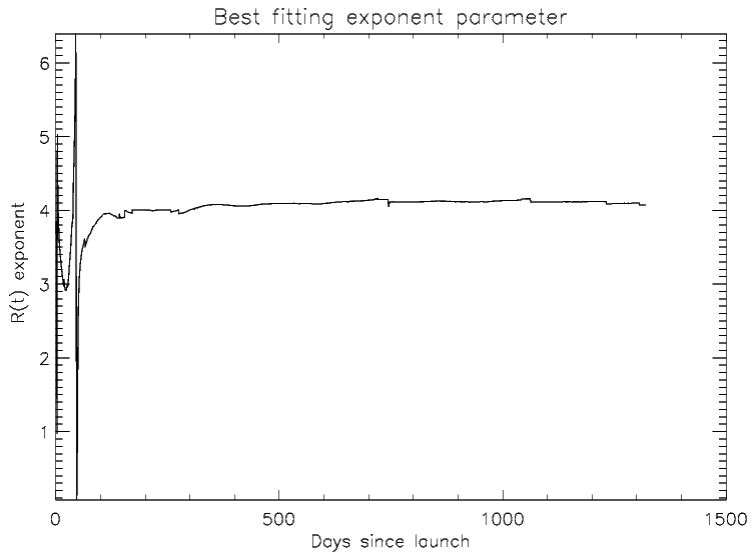

Figure 4. NOAA-20 VIIRS best fitting SRRS exponent order from the fitted H-factors.

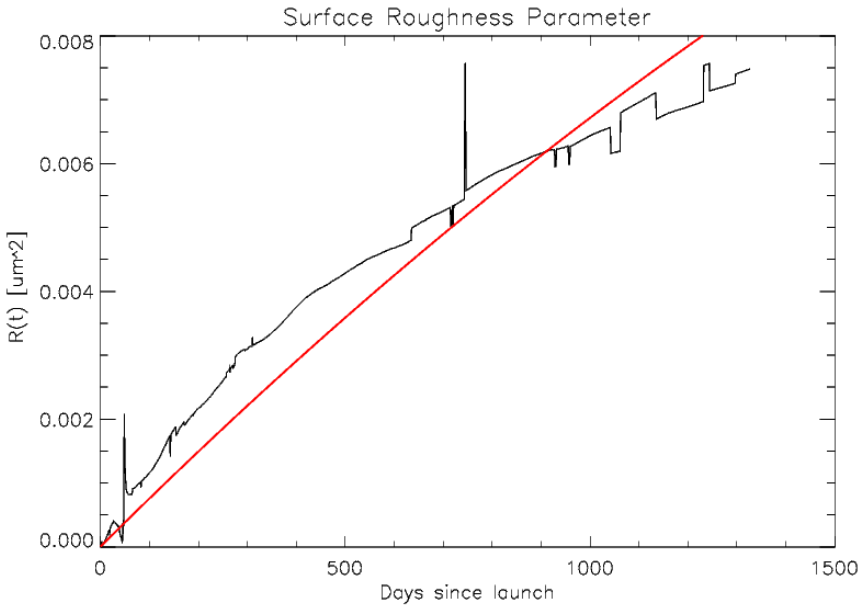

Figure 5. NOAA-20 VIIRS best fitting surface roughness R(t) [μm^2/day].

The coefficient of the surface roughness function R(t) has a very small number because the unit of the function is micrometer per day. The R(t) is forced to start at the origin point. The daily changes are very small for the SD degradation due to the surface roughness increases. The surface roughness function R(t) is very well described by the 4th order fit as shown in Figure 5.

3.2 Center Wavelength (CW) versus RSR Simulation

There are 8 detectors with the SDSM and the official SDSM center wavelengths (CWs) are being used for VIIRS SDR product in a Look-Up-Table of VIIRS-RSBAUTOCAL-H-LUT. The official NOAA-20 SDSM CW values are listed in Table 1. It should be noted that the SDSM CW is defined as double precision floating point but the values in Table 1 are defined as integers (or with 0.5 accuracy) that indicate that these CW values may not represent accurate measurements. In addition, these fixed center wavelengths were measured from the detector RSR at the center of the Full-Width at Half-Maximum (FWHM) without considering the fast degradation of the SD surface. When considering the fast non-linear degradation especially near detector 1, there could be change of the CW by altering the RSR shapes that are reflected by the SD surface.

Table 1. NOAA-20 VIIRS SDSM detector center wavelength (CW) from the VIIRS-RSBAUTOCAL-H-LUT.

Detector number	1	2	3	4	5	6	7	8
Center wavelength [nm]	411.5	448	489.5	549.5	674	744.5	868	921

Instead of using CW, the SD degradations (H-factors) can be directly measured by applying the RSR to the SRRS based simulated SD degradation. By using the SRRS model, the true SD degradation can be estimated at any wavelength of the SDSM detector RSR instead of using the CW number as shown in Table 1. Based on the current algorithm CW approach, the H-factor difference is estimated by using the SRRS model as shown in Equation 4 and 5. The CW based H-factor is calculated in Equation 6 at the official values in Table 1.

$$H_{CW}(D,t) = SRRS(CW,t) \tag{6}$$

The alternative approach is described in Equation (7) which is based on the weighted average of the SDSM RSR and SRRS model over the RSR wavelength range.

$$H_{RSR}(D,t) = \frac{\int RSR_D(\lambda) SRRS(\lambda,t) d\lambda}{\int RSR_D(\lambda) d\lambda} \tag{7}$$

If there are some out-of-band (OOB) responses or spectral leaks in the detector RSR, the H_{RSR} may have some significant time-dependent differences compared to the H_{CW}. The ratio based on the H_{CW} is measured in each detector and will be applied to the H-factor to derive HRSR for NOAA-20 VIIRS calibration.

4. RESULTS

4.1 SRRS based H-factor Algorithm Test

Using the SRRS model described by Equation 4 and 5, RSR and CW based H-factors (i.e. H_{CW} and H_{RSR}) are calculated within the SDSM detector RSR ranges. Before applying the SRRS model, the surface roughness function, R(t), is checked as shown in Figure 6 over the 10-year simulation. The R(t) is monotonically increased and saturated around 10 years of operation, which is expected by the S-NPP VIIRS SD case in the previous Shao's study [21]. The spectral range of SDSM detectors are mostly within 350 to 1200nm as shown in Figure 7. The daily SD degradation based on CW (H_{CW}) and RSR (H_{RSR}) are individually calculated by applying the quadratic function of R(t). When the reference H-factor is set and calculated from SRRS model, the H_{CW} is directly interpolated from the SRRS based H-factor as shown as dashed lines in Figure 7 and the H_{RSR} is calculated by the weighted average approach as described in Equation (6). The RSR in Figure 7 is not the true NOAA-20 SDSM RSR because they are not open to the public; however the Gaussian function based RSRs are used for visualization purposes. The actual H_{RSR} is calculated from the true NOAA-20 SDSM RSRs for the simulations

and the H_{CW} and H_{RSR} are shown in Figure 8 as dashed and solid lines, respectively. There are significant differences between the H_{CW} and H_{RSR}.

As shown in Figure 8, the rates of H-factor changes are different with the SDSM detectors. The SDSM detector 1 shows the largest time-dependent differences between the H_{CW} and H_{RSR}, whereas there were very small differences with the longer wavelength side. Please note that the direction of correction is opposite in the SDSM detector 4 in Figure 8.

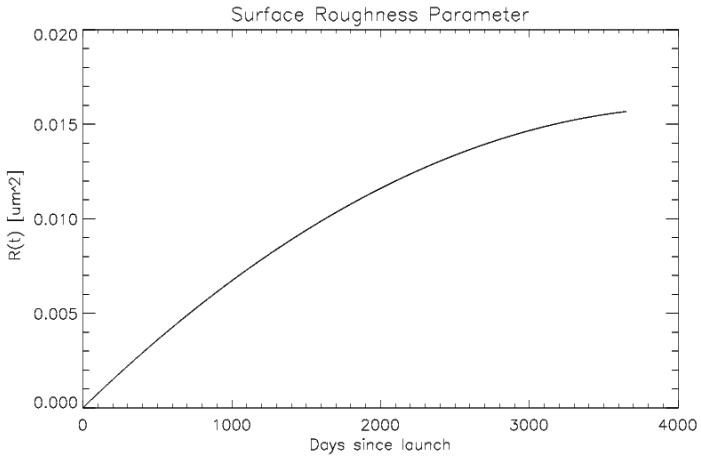

Figure 6. NOAA-20 VIIRS surface roughness R(t) [µm^2/day] over 10 years simulation.

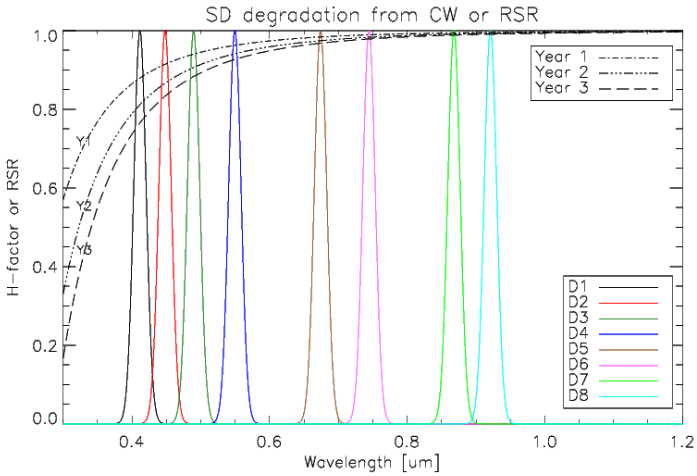

Figure 7. NOAA-20 VIIRS SDSM RSR and SRRS derived degradation. The RSR functions are derived from a Gaussian function for visualization purposes only.

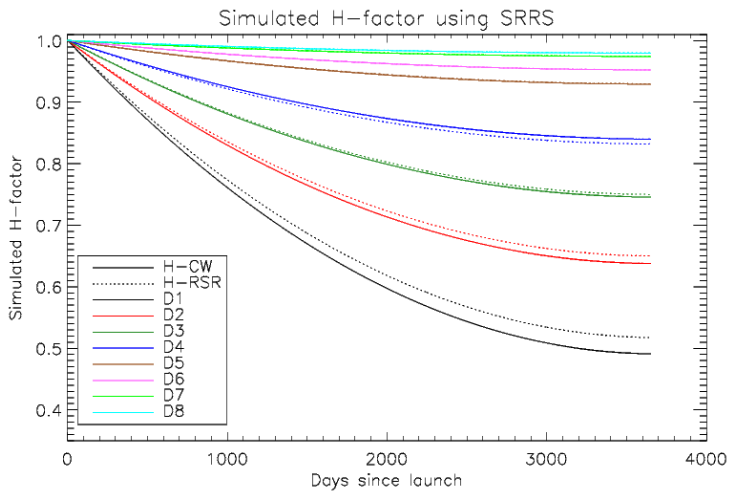

Figure 8. NOAA-20 VIIRS simulated SD degradation. Solid lines represent center wavelength SD degradation and dotted lines show the RSR weighted version from the SRRS degradation model.

Compared to H_{CW}, decreasing H_{RSR} was observed in the SDSM detector 4 which had Out-Of-Band response in the measured SDSM RSR. The measured RSR profile had constant spectral leak in the left side of the main lobe below 470 nm. After setting zero response below 470 nm with the SDSM detector 4 RSR, the H_{RSR} had a higher level than H_{CW} as shown in Figure 9. A ratio plot between H_{RSR} and H_{CW} is shown in Figure 10 as a function of H_{CW}. The effect of spectral leak is evident that the direction of correction could be changed by changing RSR shapes. The H-factor correction

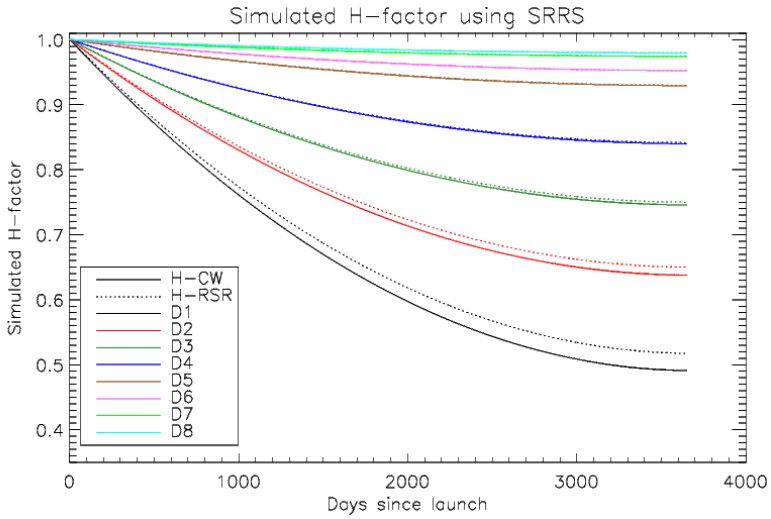

Figure 9. NOAA-20 VIIRS simulated SD degradation after removing detector 4 OOB leaks below 470nm.

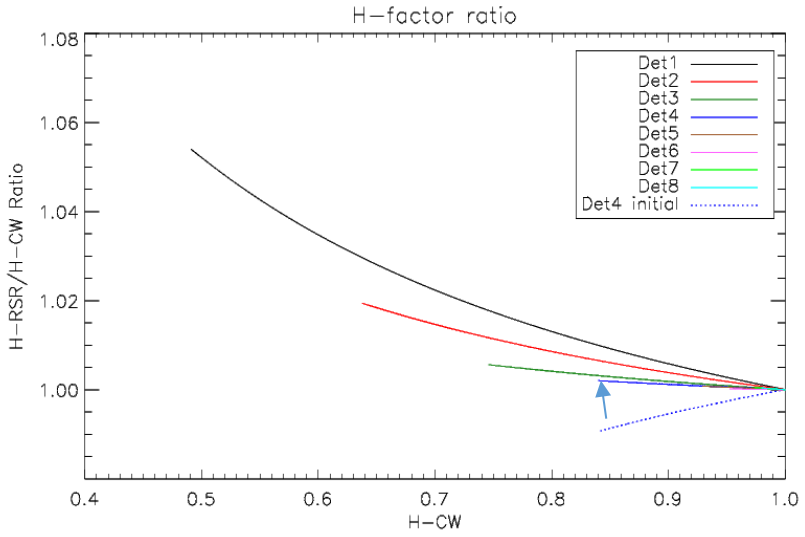

Figure 10. NOAA-20 VIIRS ratio between H_{RSR} and H_{CW} after removing detector 4 OOB leaks below 470nm. After correcting RSR OOB leak, direction of correction went to nominal trend compared to other detectors.

4.2 Applying H_{RSR} to the SD F-factors

The primary source of RSB calibration is dependent on SD observations that can be calculated every orbit. The SD F-factors are calculated and averaged daily SD F-factors as shown as solid lines in Figure 11. The SD F-factors are linearly related to any H-factor changes from Equation 2. In addition, H-factor changes directly affect the Earth view radiance in the VIIRS products. Before applying the H_{RSR}, there were differences in the long-term trends between the SD and lunar F-factors that are shown as solid lines and symbols in Figure 11, respectively. The lunar F-factors are normalized to the 2nd scheduled lunar collection on January 27, 2018 at the SD F-factor response. The annual gaps in the lunar F-factors during the summer months (June to October) are inevitable since the moon goes below the Earth limb that VIIRS cannot perform lunar observations. There are annual oscillations in lunar F-factors and SD F-factors, but the two independent F-factors are consistent within one percent level except short wavelength bands (M1-M4). The differences are growing up to 1.4 percent near days 1300 in Figure 11 in band M1.

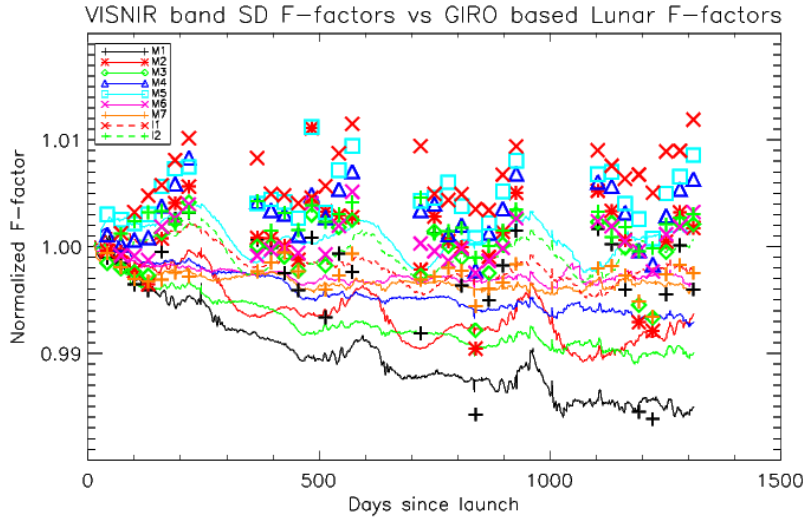

Figure 11. NOAA-20 VIIRS SD F-factors (lines) and lunar F-factors (symbols).

Figure 12 shows the newly calculated SD F-factors with H_{RSR} ratio correction. The improvements are evident in Figure 12 that the long-term trends between SD and lunar F-factors are more consistent after the H_{RSR} ratio correction especially for short wavelength bands (M1-M4). The two F-factors are very consistent within ±0.5 percent.

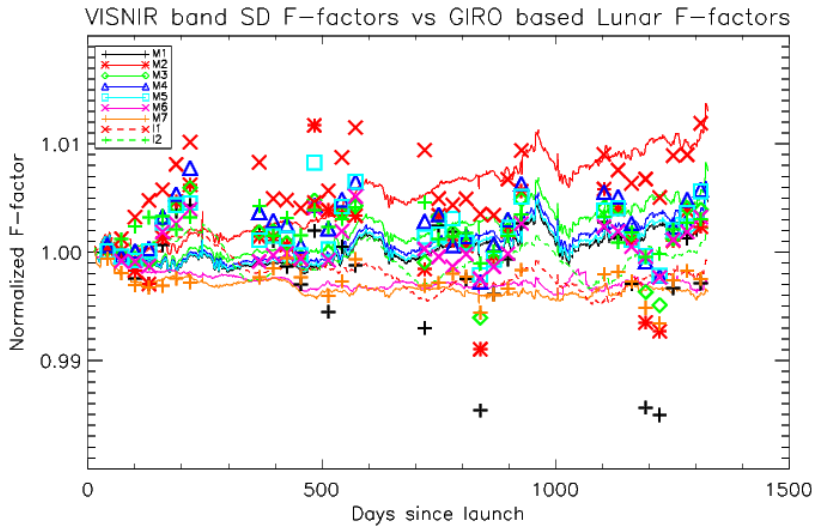

Figure 12. NOAA-20 VIIRS lunar F-factors (symbols) and SD F-factors (lines) with H_{RSR} ratio correction.

5. SUMMARY

A new version of SD degradation (H-factor) algorithm is developed and implemented to the NOAA-20 VIIRS radiometric calibration for RSB bands. There were differences between center wavelength-based H-factors and RSR derived H-factors especially in the short wavelength bands up to 1.5 percent. The OOB responses in SDSM detector RSR were the source of possible error in RSR based H-factor estimations. The NOAA-20 VIIRS SDSM detector 4 OOB leaks below 470 nm caused wrong H-factor simulation results and it was corrected by removing the OOB responses. The ratio between the center wavelength based RSR (H_{CW}) and RSR based H-factors (H_{RSR}) applied to the SD F-factors. The corrected SD F-factors were compared to the long-term trends of lunar F-factors. After the SD F-factor correction, the long-term trends between SD and lunar F-factors became very consistent from 1.5 percent difference to 0.5 percent levels. This study shows the importance of accurate SDSM detector RSR measurement especially in short wavelengths. This algorithm can be applied to JPSS-2 VIIRS SDSM RSR since there are large OOB leaks in the longer wavelength in all the SDSM detectors.

ACKNOWLEDGEMENT

Author appreciates detailed technical guidance and advice from Dr. Changyong Cao who is Satellite Calibration & Data Assimilation (SCDA) Branch Chief at NOAA STAR.

DISCLAIMER

The scientific results and conclusions, as well as any views or opinions expressed herein, are those of the author(s) and do not necessarily reflect those of NOAA or the Department of Commerce.

REFERENCES

[1] C. Cao, F. J. De Luccia, X. Xiong, R. Wolfe, and F. Weng, "Early On-Orbit Performance of the Visible Infrared Imaging Radiometer Suite Onboard the Suomi National Polar-Orbiting Partnership (S-NPP) Satellite," *IEEE Transactions on Geoscience and Remote Sensing,* vol. 52, no. 2, pp. 1142-1156, 2014.

[2] N. Baker and H. Kilcoyne, "Joint Polar Satellite System (JPSS) VIIRS Radiometric Calibration Algorithm Theoretical Basis Document (ATBD)," J. P. S. S. J. G. Project, Ed., ed. NOAA and NASA: NOAA & NASA, 2011.

[3] R. E. Wolfe, G. Lin, M. Nishihama, K. P. Tewari, J. C. Tilton, and A. R. Isaacman, "Suomi NPP VIIRS prelaunch and on-orbit geometric calibration and characterization," *Journal of Geophysical Research: Atmospheres,* vol. 118, no. 20, pp. 11,508-11,521, 2013.

[4] C. Cao *et al.*, "NOAA Technical Report NESDIS 142 Visible Infrared Imaging Radiometer Suite (VIIRS) Sensor Data Record (SDR) User ' s Guide," Sep. 10, 2013 2013.

[5] T. Choi, X. Shao, S. Blonski, and C. Cao, "On-orbit NOAA-20 VIIRS solar diffuser bidirectional reflectance distribution function and screen transmittance characterization using yaw manoeuvres and regular on-orbit SDSM data," *International Journal of Remote Sensing,* vol. 41, no. 17, pp. 6503-6526, 2020/09/01 2020.

[6] S. Lee and G. Meister, "MODIS solar diffuser degradation determination and its spectral dependency," presented at the Earth Observing Systems XXIII, 2018.

[7] R. Morfitt *et al.*, "Landsat-8 Operational Land Imager (OLI) Radiometric Performance On-Orbit," *Remote Sensing,* vol. 7, no. 2, pp. 2208-2237, 2015.

[8] T. Choi, X. Shao, and C. Cao, "On-orbit radiometric calibration of Suomi NPP VIIRS reflective solar bands using the Moon and solar diffuser," *Appl Opt,* vol. 57, no. 32, pp. 9533-9542, Nov 10 2018.

[9] J. J. Butler, E. Waluschka, J. Xiong, C. J. Bruegge, and X. Xiong, "Pre-launch optical tests of MODIS and MISR," presented at the Earth Observing Systems XIII, 2008.

[10] F. Yu and X. Wu, "Radiometric Inter-Calibration between Himawari-8 AHI and S-NPP VIIRS for the Solar Reflective Bands," *Remote Sensing,* vol. 8, no. 3, 2016.

[11] X. Shao *et al.*, "Validation of GOES-16 ABI reflective solar band calibration through reanalysis and comparison with field campaign data," presented at the Earth Observing Systems XXIII, 2018.

[12] X. Xiaoxiong, S. Junqiang, X. Xiaobo, W. L. Barnes, and V. V. Salomonson, "On-Orbit Calibration and Performance of Aqua MODIS Reflective Solar Bands," *IEEE Transactions on Geoscience and Remote Sensing,* vol. 48, no. 1, pp. 535-546, 2010.

[13] T. Choi, X. Shao, S. Blonski, W. Wang, S. Uprety, and C. Cao, "NOAA-20 VIIRS initial on-orbit radiometric calibration using scheduled lunar observations," presented at the Earth Observing Systems XXIV, 2019.

[14] T. Choi, C. Cao, and F. Weng, "RADIOMETRIC STABILITY MONITORING OF THE S-NPP VIIRS OCEAN COLOR BANDS USING THE MOON," presented at the International Symposium on Remote Sensing (ISRS), Jeju, Korea, April 20, 2016.

[15] X. Xiong, J. Sun, J. Fulbright, Z. Wang, and J. J. Butler, "Lunar Calibration and Performance for S-NPP VIIRS Reflective Solar Bands," *IEEE Transactions on Geoscience and Remote Sensing,* vol. 54, no. 2, pp. 1052-1061, 2016.

[16] J. Sun and M. Wang, "VIIRS Reflective Solar Bands Calibration Progress and Its Impact on Ocean Color Products," *Remote Sensing,* vol. 8, no. 3, 2016.

[17] X. Shao, T.-C. Liu, X. Xiong, C. Cao, T. Choi, and A. Angal, "Surface Roughness-Induced Spectral Degradation of Multi-Spaceborne Solar Diffusers Due to Space Radiation Exposure," *IEEE Transactions on Geoscience and Remote Sensing,* pp. 1-14, 2019.

[18] T. Choi, S. Blonski, X. Shao, and C. Cao, "Improving NOAA 20 VIIRS screen transmittance and solar diffuser BRF estimation from both Yaw maneuver and regular on-orbit data," in *SPIE Remote Sensing*, 2018, vol. 10785, p. 15: SPIE.

[19] T. Choi, S. Blonski, and C. Cao, "Initial on-orbit radiometric calibration of the NOAA-20 VIIRS Reflective Solar Bands," in *SPIE Optical Engineering + Applications*, 2018, vol. 10764, p. 11: SPIE.

[20] T. Choi, C. Cao, S. Blonski, W. Wang, S. Uprety, and X. Shao, "NOAA-20 VIIRS Reflective Solar Band Postlaunch Calibration Updates Two Years In-Orbit," *IEEE Transactions on Geoscience and Remote Sensing,* pp. 1-10, 2020.

[21] X. Shao, C. Cao, and T.-C. Liu, "Spectral Dependent Degradation of the Solar Diffuser on Suomi-NPP VIIRS Due to Surface Roughness-Induced Rayleigh Scattering," *Remote Sensing,* vol. 8, no. 3, 2016.

[22] C. Taeyoung *et al.*, "Suomi-NPP VIIRS Initial Reprocessing Improvements and Validations in the Reflective Solar Bands," presented at the Earth Observing Systems XXII, 104021V San Deigo, CA, 2017.